OXFORD JOURNAL
OF STUDENT
SCHOLARSHIP

Loss-Engineered Exceptional-Point Physics and Radiation-Force Particle Transport in a Sub-Wavelength Acoustic Cavity Chain

Sudhi Singh
sudhisinghhi@gmail.com

ABSTRACT

Fine particulate matter (PM2.5) is a critical air pollutant due to its ability to reach the deeper parts of the respiratory tract because of its small aerodynamic diameter (≤ 2.5 μm). Acoustic particle manipulation is a possible path to controlling airborne particles, rather than using only conventional filtration. The connection between non-Hermitian acoustic field engineering and particle-scale transport, however, is not well developed. This work aims to explore the potential of changing the acoustic spectrum, redistributing the acoustic energy, and affecting the motion of the particles in a finite chain of coupled sub-wavelength resonators with spatially graded acoustic losses.

A reduced-order framework is based on a non-Hermitian coupled-mode model, a one-dimensional interpolated acoustic pressure field, and a classical Gor'kov radiation-force potential combined with overdamped particle tracking. The two-cavity system is found to reproduce an analytical EP at r = 1, while the longer chains are found to show numerically identified pairwise EP-like candidates at r = 1. The first candidate is found close to r = 0.3254 for a ten-cavity chain, and the eigenvector overlap is greater than 0.9999. The calculated field-energy asymmetry with the increase of the loss gradient is 67.3% at r = 1.9, while the reference-particle fraction in the low-loss half only changes from 50.1% to 47.1%. The force landscape has several local reversals, which restrict the net directional redistribution. In addition, the eigenvalue gap between the first EP-like candidate grows rapidly when the frequency disorder occurs.

The results prove that the acoustic spectrum and the acoustic field distribution can be significantly changed by the loss engineering, while providing efficient particle transport is not a general rule for strong field asymmetry. Before separating the performance of PM2.5 can be realized in practice, geometry-resolved modelling and experimental validation will be needed.

Keywords: *non-Hermitian acoustics; exceptional points; coupled acoustic cavities; Gor'kov radiation force; particulate matter; acoustophoretic transport*

INTRODUCTION

Fine particulate matter (PM2.5) is an important issue in the field of air-quality management, since PM2.5 refers to particles with an aerodynamic diameter of 2.5 μm or less, which can reach the deeper parts of the respiratory system and cause adverse health effects [1]. The particles in PM2.5 are composed of a variety of chemicals, densities, shapes, and mechanical properties, which makes handling and separation of them a complex multiphase transport process. The standard fibrous filters remove particles from the air by a number of different processes, including interception, inertial impaction, diffusion, and electrostatic attraction. An alternative method is acoustic manipulation, where the forces are time-averaged forces applied by sound fields to the suspended particles. It is therefore important to understand if such forces can be controlled by engineered resonator losses for the development of alternative particle-handling concepts. A spherical particle of physical radius 1.25 μm is used here as a representative example, but is not meant to be a representative case of all atmospheric PM2.5 [2].

Particles are trapped on fibrous filters by inertial impaction, interception, diffusion, and, in some filters, due to electrostatic attraction [2]. Acoustic manipulation goes a different way. The radiation force on a particle in an imposed sound field is a time-averaged force due to the local pressure and velocity fields, as well as the acoustic contrast of the particle and the surrounding fluid [3]. It has been well-known in acoustofluidics and has been adopted for the case of airborne particles as well. Sorting airborne solid particles by the acoustic radiation force has been demonstrated using a phononic-crystal waveguide [4], while manipulation of aerosol distributions has been demonstrated using a resonant waveguide with standing-wave packets in the form of structures [5]. The results of these studies indicate that particle motion in the air can be reduced using acoustics, but the particle motion control mechanisms are not the same as the loss-engineered chain in this study.

This research aims to study the feasibility of using spatially-controlled acoustic dissipation as a passive control tool to change acoustic fields and affect the motion of fine particles in the air. The proposed framework presents a different paradigm, where the spatial distribution of cavity losses is considered as an independent design feature, as opposed to the traditional acoustic manipulation methods that are based on the geometry of the field, resonance excitation, or the formation of standing waves. The impact of this strategy is the connection between non-Hermitian spectral engineering and particle-level transport predictions, as well as characterizing when such changes in acoustic field localization can yield, or cannot yield, useful particle redistribution.

The second part is related to sub-wavelength resonant acoustics. Acoustic metamaterials and coupled resonators can modify the shape of the sound field at a size smaller than the free-space wavelength [6]. In open or dissipative systems, the effective operator is not Hermitian, and both eigenfrequencies and modes will be complex-valued and need not be orthogonal. Experimental access to exceptional points has been realized in acoustic systems that are parity-time-symmetric [9]. Later, multiple interacting EPs were shown in coupled cavities which had asymmetric losses [10]. Recently, it was also demonstrated

numerically and theoretically (via coupled-mode theory) that EPs can be generated in a single open acoustic resonator by breaking its symmetry [11].

A non-Hermitian acoustic system is a system whose effective mathematical operator contains energy exchange or dissipation and thus, in general, has complex eigenfrequencies. At an exceptional point (EP), certain parameter conditions cause two or more eigenvalues and the associated eigenvectors to merge into a single point, causing the operator to become defective. The real component of the complex eigenfrequency represents the frequency of the oscillations, and the imaginary component represents the growth or decay of the modes according to the time convention used. For this study, loss engineering means intentionally engineering how the acoustic dissipation is localized to coupled resonators. Acoustophoretic transport is the motion of a particle caused by the action of acoustic forces within the sound field.

The papers above explain both aspects of this project typically in separate contexts. Non-Hermitian acoustic work primarily focuses on the study of spectral coalescence, scattering, sensing, and wave control, while the study of particle manipulation focuses on the forces and motion that a particular acoustic field produces. A study starting with a passively loss-graded finite acoustic cavity chain, through pairwise near-coalescence, Gor'kov radiation force, and the trajectory of the airborne particles on the PM-scale, was not found in the literature reviewed here. This study shows one of the calculations from the loss gradient to the spectrum, the driven field asymmetry, the force landscape, and particle trajectories. The chain-length and disorder tests are employed to ascertain the degree of dependence of the spectral result on the selected finite system.

The present study aims to answer three questions: (i) What is the effect of a spatial loss gradient on the eigenvalue spectrum and the generation of pairwise EP-like behavior in finite acoustic cavity chains? (ii) What is the effect of the acoustic field asymmetry due to the loss on the radiation-force landscape and particle trajectories? (iii) How sensitive are these predictions to the particle properties, the amount of disorder in the cavity frequencies, and the chain length? The working hypotheses are that as the asymmetry of the loss increases, the spectrum becomes near-coalesced and the number of trapped particles is redistributed in space; however, these changes do not necessarily lead to proportional change in the direction of the particle transport, as more than one local trapping region may exist in the force landscape. These hypotheses are tested with a reduced-order numerical model instead of a geometry-resolved or experimentally validated separator.

THEORETICAL BACKGROUND

The theoretical approach is developed in five steps to relate the acoustic characteristics of the resonator chain with the foreseen motion of airborne particles. First, the complex eigenfrequency of a single dissipative cavity is introduced to explain how dissipation enters into a non-Hermitian description. Second, the two coupled cavities are investigated to determine the analytical point of the exception. Third, the model is generalized to the case of a finite chain with a spatially varying loss. Fourth, the driven cavity amplitudes are converted into a continuous approximate pressure and velocity field. Last, the

radiation-force potential is calculated, along with the overdamped particle trajectories, which are used to make the acoustic field. This development helps to distinguish the spectral characteristics of the unforced system from the particle motion induced by the acoustic response of the driven system.

For one cavity with bare angular resonance ω_0 and amplitude-decay rate γ, the freely decaying complex modal amplitude is

$$\frac{da}{dt} = \left(-\, i\omega_0 - \gamma\right)a.$$

The complex eigenfrequency can be expressed as $\lambda = \omega_0 - i\gamma$, where $\mathrm{Re}(\lambda) = \omega_0$ represents the frequency of oscillations, and $\mathrm{Im}(\lambda) = -\gamma$ represents exponential decay. The simplest way the loss term becomes part of the effective non-Hermitian description of an open resonator is [8].

Two identical resonators coupled with strength J and allowed to have different losses are represented by

$$H = \left(\omega_0 - i\gamma_1\, J\, J\, \omega_0 - i\gamma_2\right).$$

With $\gamma^- = \left(\gamma_1 + \gamma_2\right)/2$ and $\Delta\gamma = \left(\gamma_1 - \gamma_2\right)/2$, the eigenvalues are

$$\lambda_\pm = \omega_0 - i\gamma^- \pm \sqrt{J^2 - (\Delta\gamma)^2}.$$

If the value of r is defined as r=/J, the analytic dimer EP will be defined at r=1. The real parts are divided below this, and the decay rates are the same. Above that, the real parts join together, and the decay rates are divided. The two eigenvalues and eigenvectors of the EP merge [8]. This eigenvector-matrix condition number is not used as a measure of particle transport, but instead as a numerical check on the dimer singularity.

The Hamiltonian for N nearest-neighbour coupled cavities is tridiagonal. The diagonal terms (0−in) are set to 0, while the adjacent cavities are connected with J. A linear loss gradient is applied as:

$$\gamma_n = \Gamma_0 + rJ\left(1 - \frac{2(n-1)}{N-1}\right), \qquad n = 1, \ldots, N,$$

with $\Gamma_0 = 2J$. This simplifies to the dimer definition when N=2. For larger systems, the different eigenvalues may be converging at different r values, as can happen in multi-state non-Hermitian systems [10]. Therefore, the finite-chain calculation does not consider one particular analytic EP. It looks at local minima of the smallest pairwise gap of eigenvalues, and examines the overlap of the eigenvectors corresponding to those eigenvalues.

The free modes are described by the eigenvalue problem. The forced steady state determines the motion of particles. All cavities are driven at ω_0. Writing $a_n(t) = A_n e^{-i\omega_0 t}$ gives

$$(\Gamma + iJC)A = -is_0 1,$$

where $\Gamma = diag(\gamma_n)$ and C is the nearest-neighbour adjacency matrix.

The discrete values of the cavity amplitudes are not sufficient to describe a continuous pressure field between the cavity centres. The following report is thus based on a Gaussian interpolation,

$$p(y) = N \sum_{n=1}^{N} A_n exp\left[-\frac{(y-y_n)^2}{2\sigma^2}\right],$$

with $\sigma = 0.5$ mm. The scalar N is chosen so that $max|p| = 400$ Pa. The Gaussian profile and the peak of 400 Pa are modelling options. The first is a spatial basis for associating the discrete chain with a continuous one-dimensional field; the second is only a scale for the overall force. It is not actually a measured pressure from a manufactured instrument; it is not the dimensionless drive amplitude in the coupled mode equation.

For the $e^{-i\omega_0 t}$ convention, the inviscid linearized momentum equation gives

$$v(y) = \frac{1}{i\omega_0\rho_0}\frac{dp}{dy}.$$

For a small spherical particle, the classical Gor'kov potential and radiation force are [12]

$$U(y) = \frac{4\pi a^3}{3}\left[\frac{f_1}{2\rho_0 c_0^2}\langle p^2\rangle - \frac{3f_2\rho_0}{4}\langle v^2\rangle\right], \qquad F_{rad}(y) = -\frac{dU}{dy}.$$

The contrast factors are

$$f_1 = 1 - \frac{\kappa_p}{\kappa_0}, \qquad f_2 = \frac{2(\rho_p - \rho_0)}{2\rho_p + \rho_0}.$$

With Stokes drag $\zeta = 6\pi\mu a$, the overdamped particle equation is

$$\zeta\frac{dy}{dt} = F_{rad}(y).$$

Within this particular reduced model, $F_{rad} \propto a^3$ and $\zeta \propto a$, so the settling time scales as $T \propto a^{-2}$. This scaling is not an independent prediction from experiment but rather is a property of the equations used. Acoustic radiation forces on small particles might change with viscous corrections [13]. The force may also be affected by the thermoviscous effects [14]. There can be a competing drag contribution due to acoustic streaming [15].

METHODOLOGY

A one-dimensional reduced-order model is considered in this study. The purpose is not to duplicate the entire flow and pressure distribution in a complete geometry of the separator. In contrast, the model will focus on one question: If the cavity losses are intentionally made asymmetric, what happens to the spectrum, driven field, and particle-force landscape in the same calculation?

Model parameters

The parameters used in the main ten-cavity calculation are shown in Table I. One of the acoustic-contrast pairs is defined by the reference particle density and compressibility. The particle bias is not a direct measurement of atmospheric PM2.5, and thus the direction of the calculated bias should not be interpreted as a universal one.

Table I. Parameters used in the ten-cavity reduced-order model

Quantity	**Symbol**	**Value**
Bare cavity resonance	f_0	20 kHz
Number of cavities	N	10
Cavity pitch	d	1.0 mm
Gaussian mode width	σ	0.5 mm
Air density	ρ_0	1.2 kg/m^3
Speed of sound	c_0	343 m/s
Nearest-neighbour coupling	J	100 pi ≈ 314 rad/s
Mean loss	Γ_0	2J ≈ 628 rad/s
Maximum loss-asymmetry ratio	r_{max}	1.9

Quantity	**Symbol**	**Value**
Peak interpolated pressure	–	400 Pa
Reference radius	a	$1.25\ \mu m$
Particle density	ρ_p	1000 kg/m^3
Assumed particle compressibility	κ_p	2.5 × 10^-11 Pa^-1
Compressibility contrast	f_1	1.000 (approx.)
Density contrast	f_2	0.998
Air dynamic viscosity	μ	1.81 × 10^-5 Pa s

The model parameters were chosen to represent a typical sub-wavelength coupled-resonator structure, not to be the replica of a fabricated device. The chosen cavity pitch of 1 mm is much smaller than the resonance wavelength (acoustic frequency of 20 kHz is equivalent to a resonance wavelength of 17.2 mm in air). A ten-cavity configuration enables an investigation of multiple modes interacting with each other and with different losses in a spatially graded system, and retains a manageable computational complexity. The Gaussian width value of 0.5 mm is a parameter that is assumed for interpolation and is used to specify the amount of spatial overlap between neighboring cavity contributions.

The frequency scale for inter-cavity interactions is set by the coupling strength J = 100π rad/s, and the baseline dissipation is set by the mean amplitude-decay rate $\gamma_0 = 2J$. The ratio of the loss asymmetry r is varied in the range from 0 to 1.9, which includes the analytically known dimer EP at r = 1 and the numerically determined EP-like candidates that come from finite chains. The linear loss profile assumed gives the smallest damping rate as $\gamma_0 - rJ$, which is always positive in this range. The value of the pressure amplitude is normalized rather than measured to a selected operating pressure for the convenience of comparing to other pressures.

At 20 kHz, $\lambda = c_0/f_0 \approx 17.2$ mm, giving $d/\lambda \approx 0.058$. The array is therefore sub-wavelength at the chosen frequency.

Numerical procedure

First, the dimer is compared with its analytic eigenvalues. For finite chains N>2, candidate near-coalescent states were determined by minimizing the separation of complex eigenvalues between pairs of modes, calculating the normalized overlap of the right eigenvectors of the complex eigenvalues. The pairwise eigenvalue gap showed a local minimum, and the eigenvector overlap was greater than 0.9999; in those cases, the candidate was classified as EP-like. This criterion is an operational numerical criterion for near-coalescence that is not necessarily a mathematical proof of an exceptional point. For exact confirmation of the EP, an eigenvalue degeneracy analysis would have to be carried out in addition to geometric and algebraic multiplicity analysis and defectiveness of the system matrix analysis. By this means, the finite-chain results are always referred to as EP-like candidates, and the analytically proved dimer singularity at r = 1 is called an exact EP.

The model also checks the exactly symmetric case at $r = 0$ and verifies the internal size scalings $F \propto a^3$ and $T \propto a^{-2}$.

The continuous field is sampled at 1200 equally-spaced points between 0 and 9 mm. Once the Gaussian superposition is created, it is re-scaled to the 400 Pa peak mentioned above. The harmonic momentum relation is then used to calculate the acoustic velocity, prior to the calculation of the Gor'kov potential and force.

The number of initial particle positions is 5000 with a fixed random particle seed of 0, and the initial particle positions are drawn once from a uniform distribution between 0.02 mm and 8.98 mm for the directional-collection calculation. The same starting positions are repeated for each value of r; thus, variations in the collection curve are not due to a different random sample. The overdamped equation is solved using an explicit Euler time step. The timestep is determined by

$$\Delta t = 0.06 \frac{\zeta d}{max|F_{rad}|},$$

The collection sweep is not using a fixed timestep for all r, but rather a new one is calculated each time, based on the force landscape of that specific r run. The same procedure is applied to the particle-size settling calculation, with Δt being re-calculated for each radius. This ensures that the steps' displacement is smaller than one cavity pitch. The number of integration steps per collection run is 5000, and the positions are restricted to the modelled interval if the update is beyond the interval boundaries. The last reported number is the percentage of particles that end up to the left of the middle of the array.

The settling-time calculation considers a particle to be settled if the magnitude of the local force is less than 10^{-3} of the peak force in the landscape. You can take a maximum of 20,000 steps. These details are included to influence the reported times as well as to produce the same trajectory from the program.

Fabrication disorder is represented by independent cavity-frequency offsets $\delta\omega_n \sim N\left(0, (\epsilon J)^2\right)$. At each disorder level, the minimum eigenvalue gap is averaged over 60 realizations. The comparison is made both at $r = 1$ and at the first ten-cavity EP-like point.

A separate material-sensitivity check varies the density-contrast factor f_2 while holding the same $r = 1.9$ acoustic field and $f_1 \approx 1$ fixed. It is not intended as a database of real aerosol materials. Its purpose is simply to test whether the sign of the collection bias depends on the assumed particle contrast.

RESULTS

Spectral results

The numerical dimer is used to simulate the analytic square-root transition. The two branches of the eigenvalues become coincident at r=1 in the complex plane (see Fig. 1). The same value is used for the frequency splitting and for the decay-rate splitting in Fig. 2. The eigenvector overlap is equal to one at the transition (Fig. 3), and the condition number of the eigenvector matrix increases rapidly (Fig. 4). This is a benchmark to be applied to the larger chains before using the same numerical machinery.

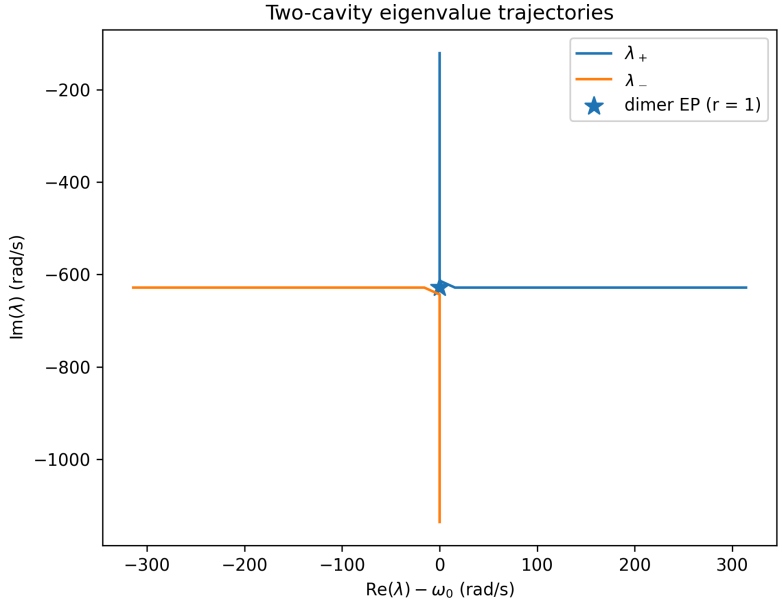


Fig. 1. Complex eigenfrequency trajectories of the two-cavity non-Hermitian model as the normalized loss-asymmetry ratio r is varied. The marker identifies the analytical EP at $r = 1$, where the eigenvalues coalesce.

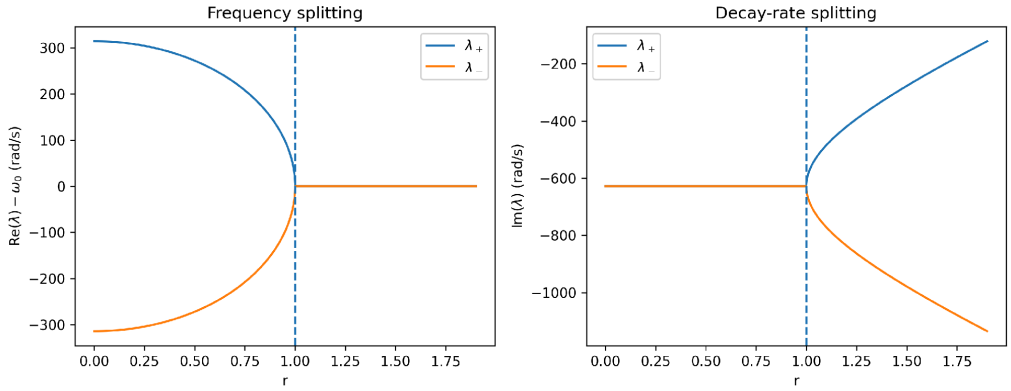


Fig. 2. Splitting of the real and imaginary components of the two dimer eigenfrequencies as a function of r. The transition at $r = 1$ separates the regimes of real-frequency and decay-rate splitting.

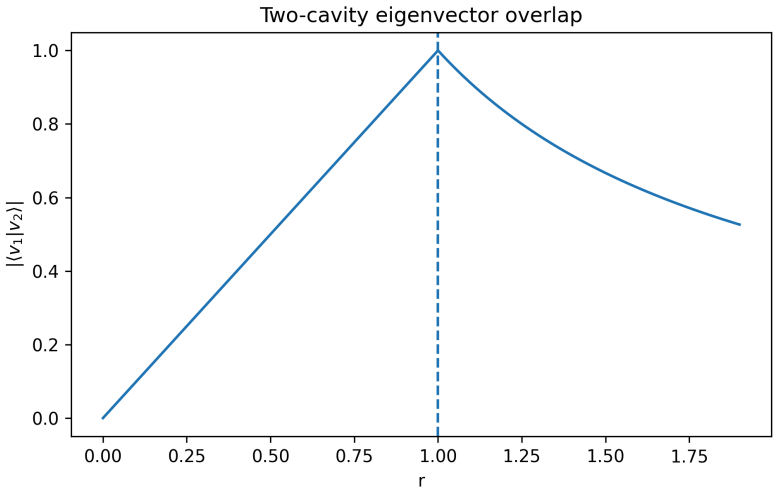


Fig. 3. Normalized overlap between the two right eigenvectors of the acoustic dimer as a function of r. An overlap approaching unity indicates eigenvector coalescence near the analytical EP.

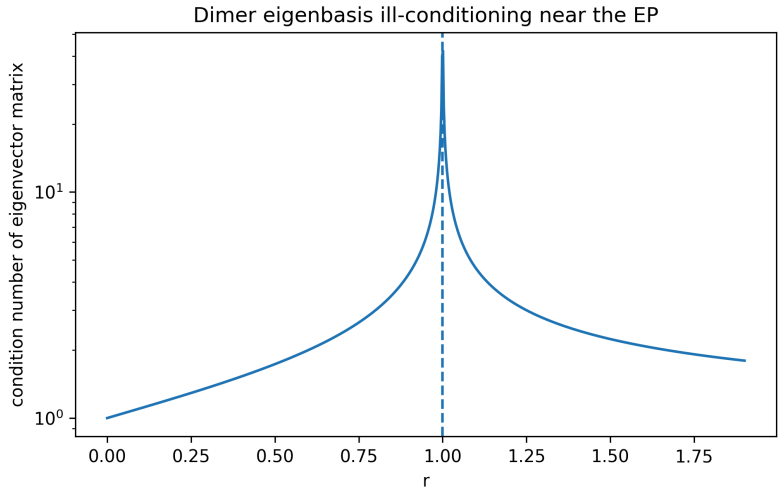


Fig. 4. Condition number of the dimer eigenvector matrix as a function of r, illustrating increasing numerical ill-conditioning near the analytical EP at $r = 1$.

The following pairwise EP-like point is very sensitive to the chain length (Table II and Fig. 5). The four-cavity chain first starts to move slightly above the dimer value, and then the first threshold drops as the number of cavities increases. The first candidate is at r=0.3254, when N=10. The minimum pairwise gap is 0.0118 rad/s, and the best overlap between the eigenvectors is >0.9999. A second candidate of high overlap shows up near r=1.308. The chain-length plot is used only for the first candidate, and the same definition is used for all N.

Table II. First pairwise EP-like point versus chain length

N	$r_{EP-like,1}$	**Minimum gap (rad/s)**	**Closest-pair overlap**
2	1.0000	0.0269	0.99999
4	1.0607	0.0244	0.99999
6	0.6787	0.0191	0.99999
8	0.4569	0.0130	0.99999
10	0.3254	0.0118	0.99999

N	$r_{EP-like,1}$	**Minimum gap (rad/s)**	**Closest-pair overlap**
14	0.1873	0.00130	0.99999
20	0.1004	0.00244	0.99999

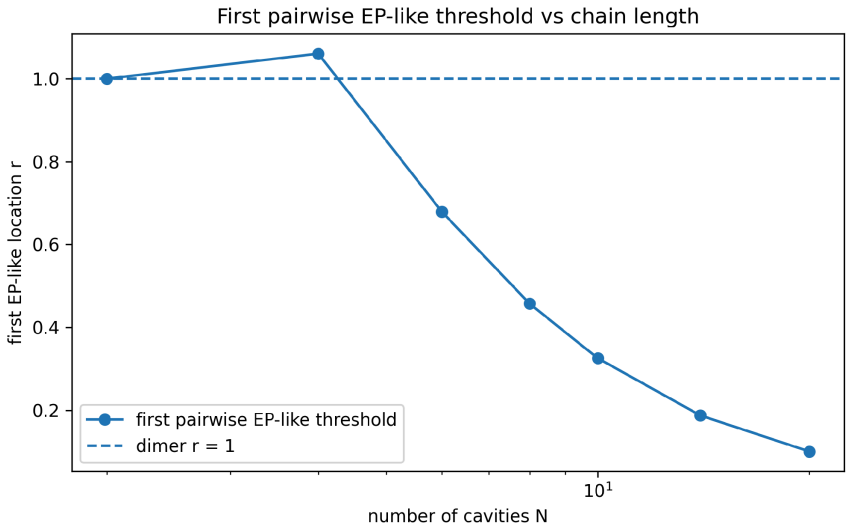


Fig. 5. Normalized loss-asymmetry ratio of the first numerically identified EP-like candidate as a function of cavity-chain length N. The dashed line indicates the exact dimer EP at $r = 1$.

4.2 Driven field and particle transport

Symmetrical driving results in uniform energy distribution at r=0. The loss gradient decreases as the loss increases, and the energy imbalance is almost linearly related to the loss over the tested range. It is about 12% near the first ten-cavity EP-like point, about 36% at r=1, and 67.3% at r=1.9 (Fig. 6). The curve is not maximal around r=0.325. In this model, the field asymmetry is therefore primarily due to the imposed loss gradient of the driven chain rather than to a dramatic enhancement which is localized at the first EP-like point.

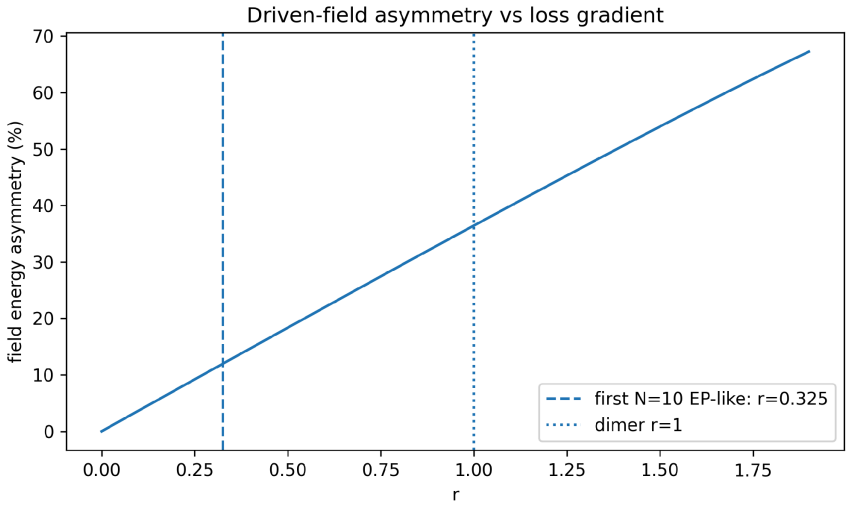


Fig. 6. Driven-field energy asymmetry of the ten-cavity chain as a function of normalized loss-asymmetry ratio. The dashed and dotted lines indicate the first ten-cavity EP-like candidate and the analytical dimer EP, respectively. The definition of energy asymmetry should be provided in the figure or caption.

For the reference particle, the peak force magnitude is about 31.1 fN at r=0, 30.9 fN at r=0.325, and 37.8 fN at r=1.9. The number of zero-crossing points of the respective curves is 29, 27, and 21 (Fig. 7). Stability of a zero crossing does not follow automatically; the direction of the force on each side dictates stability. The key point here is how many local reversals there are within the landscape in just 9 mm.

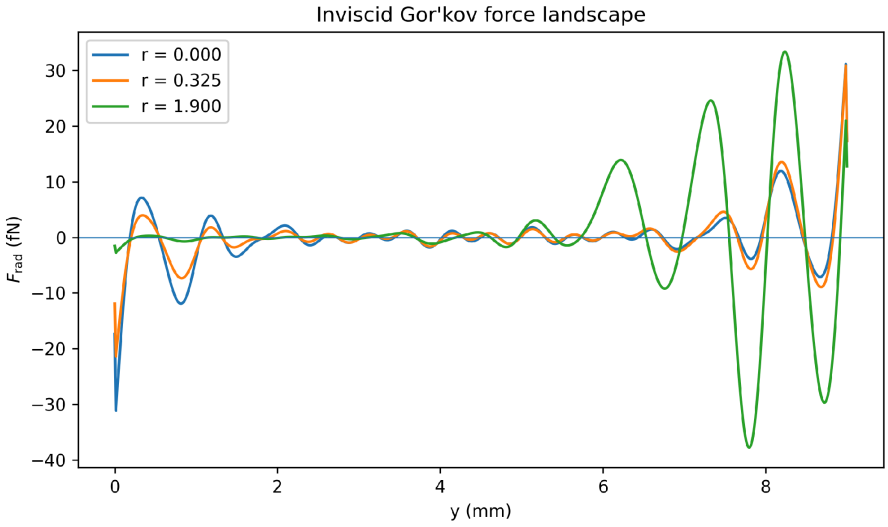


Fig. 7. One-dimensional acoustic radiation-force profiles calculated using the inviscid Gor'kov formulation for a reference particle of radius 1.25 μm at $r = 0, r = 0.3254$, and $r = 1.9$. Positive and negative forces indicate opposite directions along the cavity-chain coordinate.

The size sweep shows the typical a-2 scaling of the model used (Fig. 8). For the chosen initial point, representative radii of r=0.40, 1.25, and 5.00 m settle down to the same grid-resolved equilibrium position (r=0.3254) on very different timescales (Table III). It takes approximately 194 s for the reference PM2.5 particle.

Table III. Representative settling times near the first $N = 10$ EP-like point

Particle label	**Radius (um)**	**Final position (mm)**	**Settling time (s)**
PM1	0.40	4.712	1895
PM2.5	1.25	4.712	194
PM10	5.00	4.712	12.1

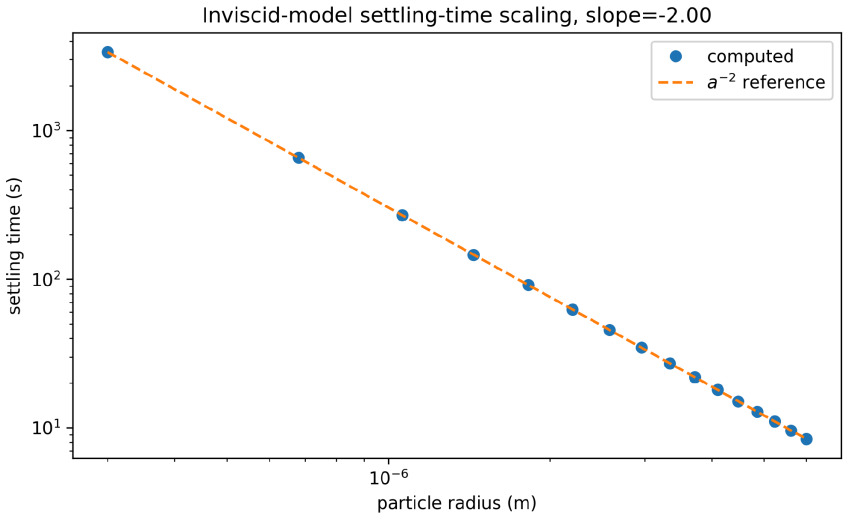


Fig. 8. Calculated settling time as a function of particle radius near the first ten-cavity EP-like candidate. The trend follows the a^{-2} scaling of the adopted overdamped radiation-force model.

The final particle distribution is compared to the field-scale asymmetry in Figure 9. At the end of the sweep, 50.1% of the simulated particles are collected in the low-loss side, while 47.1% are collected in the high-loss side. The field-energy asymmetry increases from 0% to 67.3% in the same range. At the first EP-like point, there is no jump or local maximum in the particle curve. The final distribution is changed by the loss gradient, but the response of the particles is far weaker than the field-loss imbalance.

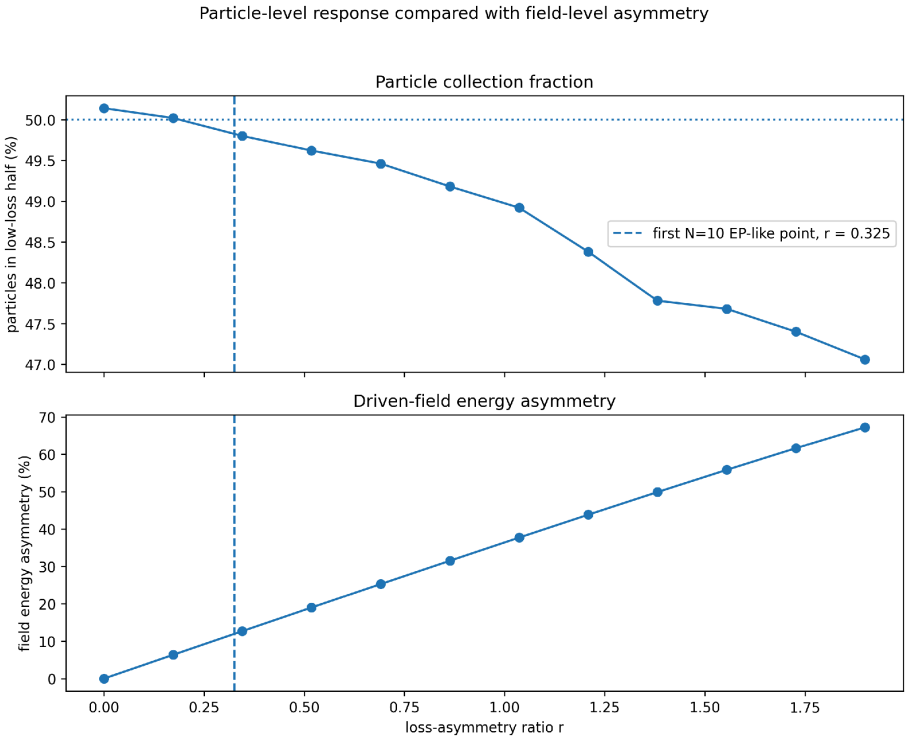


Fig. 9. Comparison of acoustic field-energy asymmetry and the percentage of reference particles ending in the low-loss half of the ten-cavity chain as a function of r. All simulations use the same 5,000 initial particle positions.

The asymmetry between the field-energy distribution and the fraction of particles collected can be explained by the spatial structure of the landscape of radiative forces. The loss gradient converts acoustic energy between the two parts of the chain, while the Gor'kov force is proportional to the spatial derivative of the local acoustic potential. However, it is not a necessary condition for a globally asymmetric field to generate a unidirectional force over the cavity chain. The force is oscillating in sign (as displayed in Figure 7), thereby establishing a number of local trapping regions. Particles then drift towards nearby equilibrium positions, instead of moving steadily towards the low-loss side. This is why the significant amount of field-energy asymmetry is associated with a relatively small change in the resulting particle distribution.

Robustness and material sensitivity

The location of the clean system greatly affects the disorder response. The ten-cavity chain is not close to its first pairwise coalescence at r=1, and the mean minimum gap varies slightly with the introduction of random frequency offsets. At r=0.3254, the clean gap is only 0.0118 rad/s. At a scale of 0.5%, the mean gap is approximately 14.5 rad/s, and at 5% the mean gap is approximately 45.3 rad/s (Table IV and Fig. 10). So, near-coalescent pairs can be easily separated from each other by cavity detuning.

Table IV. Mean minimum eigenvalue gap under frequency disorder (60 realizations per point)

Evaluation point	**0%**	**0.5%**	**1%**	**2%**	**3%**	**5%**
$r = 1$	128.2	123.0	118.1	110.8	109.4	109.3
$r = 0.3254$	0.0118	14.5	20.5	28.9	35.3	45.3

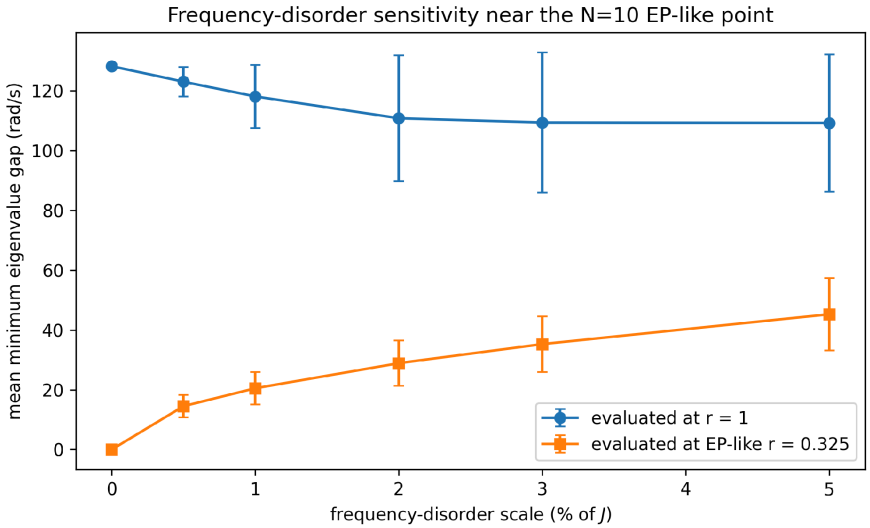


Fig. 10. Mean minimum pairwise complex-eigenvalue gap as a function of cavity-frequency disorder for the ten-cavity chain, evaluated at $r = 1$ and $r = 0.3254$. Error bars represent the standard deviation over 60 independent disorder realizations.

The collection bias should not be determined solely by the loss gradient. If r1=1.9 and f2 is changed, the number of particles received by each half changes (Fig. 11). The low-loss side will have a higher percentage of particles for some contrast values, and a lower percentage of particles for the listed reference contrast value. This is because the 47.1% result represents a result for the assumed particle properties only and not a general prediction for all PM2.5 aerosols.

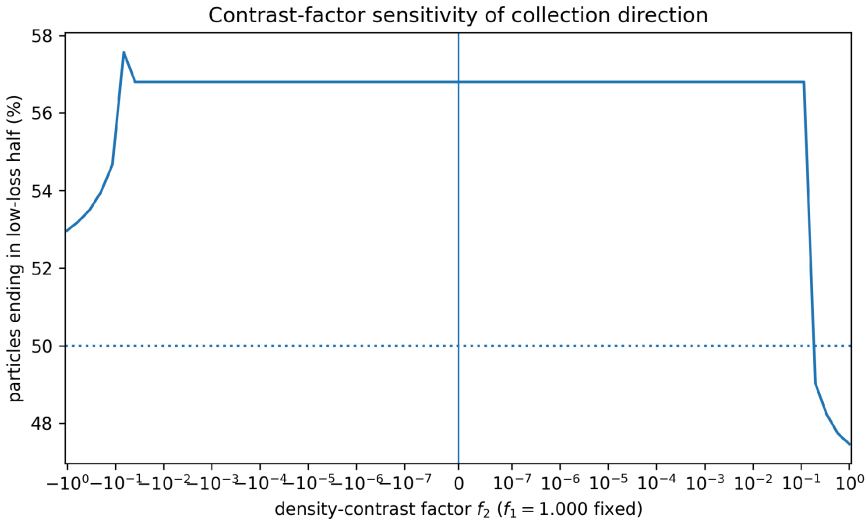


Fig. 11. Sensitivity of the final particle distribution to the assumed density-contrast factor f_2 at $r = 1.9$, with f_1 held approximately equal to unity. The results illustrate material-dependent changes in the predicted collection direction.

DISCUSSION

The forced field becomes more asymmetric, and the spectrum of the finite chain states becomes pairwise near-coalescent as r is increased. The peaks of these trends do not coincide. The first EP-like point occurs at r=0.325, and the field asymmetry is the greatest at the highest gradient value tested in the 10-cavity model. The first EP-like point does not maximize the particle bias, either.

The small particle response is explained with the help of the force landscape. Figure 7 has a lot of force reversals and local basins, so a particle will tend to head for one of the nearby basins of equilibrium rather than the entire array. Even for a high field-energy asymmetry as low as 67.3%, the final field-energy distribution changes by only three percentage points from 50:50. The net redistribution is minimal and is not considered an efficient bulk redistribution method.

Another drawback is the absolute time scale. The chosen PM2.5 trajectory reaches the first ten-cavity EP-like point around 194 s, and smaller particles take longer in the selected model. The geometry, more usable fields, longer residence time, background flow to account for the force landscape, or other transport mechanisms would be needed for a practical separator. This calculation does not demonstrate that the aforementioned engineering requirements are already addressed.

Practical Implications and Experimental Validation

The results indicate that the acoustic response of the coupled resonators can be altered even without tuning the nominal cavity resonance frequencies through the spatial loss engineering technique. However, the present calculations do not show the efficient separation of particles according to their sizes. The relatively low redistribution of reference particles, along with the multiple local force equilibria, suggests that more design optimization is required.

Validation of experiments could be done in several steps. A finite string of acoustically coupled cavities, as well as dissipation elements, could be produced with an adjustable loss gradient, which is the first step. The complex modal response and driven-field asymmetry could then be characterized by frequency-response measurements and spatial pressure mapping. Second, the independent characterization of the size, density, and compressibility of the particles could be introduced into the acoustic region, and their trajectories could be recorded by using the optical particle-tracking technique.

Acoustic measurements should be performed with both symmetric and loss-graded set-ups while maintaining a controlled acoustic excitation, concentration of particles, and airflow. The collection fraction, the velocity of particle transport, the residence time of particles, and the size-dependent separation efficiency should be numerically determined. Geometry-resolved simulations done in parallel with thermoviscous losses, acoustic streaming, and the appropriate models for particle drag would aid in delineating radiation-force effects from fluid-mediated transport. When these simulations agreed with measurements, the feasibility of loss-engineered acoustic particle separation could be verified only then.

The “chain-length” result is easier to interpret on the non-Hermitian side. The actual dimer EP is located at r=1, and the first ten EP-like points are located close to r=0.325, and another candidate with high overlap is close to r=1.308. More than one near-coalescent point, in pairs, has already been observed in multi-cavity acoustic systems, so more than one pairwise near-coalescent point in a larger chain is not unexpected. When calculating, the first threshold also moves depending on the finite-chain loss profile.

The disorder sweep is also important since it checks the robustness of the small clean spectral gap. It is not: detuning quickly unfolds the near-coalescent pair of cavity frequencies. The fragility would have to be taken into account in any physical realization that does not allow the realization of the same resonator frequencies.

As stated in the Introduction, acoustic sorting has been shown in a phononic waveguide and aerosol redistribution has been shown in resonant standing-wave fields in previous airborne studies. In this study, the question is how much of the field asymmetry (due to the same loss parameter) that reorganizes the non-Hermitian spectrum will manifest in the particle trajectories. The reduced model makes the assumption that only a small proportion of the field-level asymmetry is manifested as net particle bias.

LIMITATIONS

In the present investigation, the acoustic cavity chain is reduced to a one-dimensional representation. This can be done within a unified computational framework to consider the spectral response, the acoustic field distribution, and the particle dynamics, but there are several effects that are not explicitly resolved.

First, the classical Gor'kov potential is calculated by applying the inviscid approximation. Viscous and thermal effects can alter the acoustic scattering response and the resulting radiation force for micrometer-sized airborne particles. As such, the force magnitudes and equilibrium positions calculated in this work may be different from those obtained via a thermoviscous formulation.

Second, acoustic streaming is not included. An acoustic radiation force may be counteracted or augmented by an extra drag force that may be induced by the streaming motion of the fluid. The forces calculated are on the order of tens of femtonewtons, and so the effect of streaming cannot be neglected without a more quantitative evaluation.

Third, particles are assumed to be spherical and have constant material properties. The particle-particle interactions, aggregation, shape variations, and PM2.5's heterogeneous composition are ignored. The other effects of background flow, Brownian diffusion, wall interactions, and slip-corrected drag are also neglected. Such effects may change the direction and scale of particle transport.

Last but not least, Gaussian pressure-field interpolation is not a "geometry-resolved" acoustic solution, and peak pressure of 400 Pa is assumed as normalization and not an experimentally proven working condition. Hence, the results do provide trends in the adopted model, but are not sufficient to conclude on the separation efficiency of the physical device.

CONCLUSION

In this work, the effect of the spatially graded acoustic losses on the spectral properties, driven acoustic fields, and particle transport due to the radiation force of a finite sub-wavelength acoustic cavity chain has been investigated. An interpolated pressure field, the classical Gor'kov radiation-force formulation, and overdamped particle tracking were integrated with a reduced-order non-Hermitian coupled-mode model.

The two-cavity model resulted in the analytically found EP at $r = 1$. For longer chains, eigenvalue-gap and eigenvector-overlap analysis based on numbers revealed EP-like candidates that clearly depend on the chain length. The first candidate appeared in the ten-cavity system close to $r = 0.3254$, and the value of the gap between its eigenvalues was very small and was very sensitive to the presence of disorder in the cavity frequencies.

The driven acoustic field was significantly modified by increasing the loss gradient to obtain a maximum calculated field-energy asymmetry of 67.3% at $r = 1.9$. This strong field redistribution did not give rise to a similar particle-level response. The percentage of reference particles that were collected and labeled in

the low-loss half was reduced from 50.1% to 47.1%, with confirmation of the collection-side labelling. The multiple reversals of the radiation-force landscape account for the observed lack of sustained direction in radiation-force transport of particles. The settling time of about 194 s for the particle used as the reference further demonstrates the shortcomings of the modeled transport mechanism.

The results demonstrate that passive loss engineering can be used to control the non-Hermitian acoustic spectra and the spatial force distributions, but neither the spectral near-coalescence nor the strong acoustic field asymmetry itself is sufficient to ensure efficient particle separation. The results are not a validated separation device, but provide a theoretical foundation for further study. Some of the directions for future work include the incorporation of geometry-resolved acoustic fields, thermoviscous effects, acoustic streaming, realistic particle drag, and controlled experimental measurements to evaluate whether loss-engineered cavity chains can separate particles by useful size and/or material.

REFERENCES

[1] U.S. Environmental Protection Agency, “Particulate Matter (PM) Basics,” last updated May 21, 2026. Accessed: Aug. 17, 2026. Available: https://www.epa.gov/pm-pollution/particulate-matter-pm-basics

[2] L. Brosseau and R. Berry Ann, “N95 Respirators and Surgical Masks,” NIOSH Science Bulletin, Centers for Disease Control and Prevention, Oct. 14, 2009. Accessed: Aug. 17, 2026. Available: https://www.cdc.gov/niosh/bulletin/2009/respirators-and-masks.html

[3] H. Bruus, “Acoustofluidics 7: The acoustic radiation force on small particles,” Lab on a Chip, vol. 12, pp. 1014-1021, 2012, doi: 10.1039/C2LC21068A.

[4] N. Korozlu, A. Biçer, D. Sayarcan, O. A. Kaya, and A. Cicek, “Acoustic sorting of airborne particles by a phononic crystal waveguide,” Ultrasonics, vol. 124, 106777, 2022, doi: 10.1016/j.ultras.2022.106777.

[5] Z. Qiao, Y. Huang, V. Naso, and W. Dong, “Aerosol manipulation through modulated multiple acoustic wavepackets with a pair of resonators,” Powder Technology, vol. 322, pp. 24-31, 2017, doi: 10.1016/j.powtec.2017.08.062.

[6] S. A. Cummer, J. Christensen, and A. Alù, “Controlling sound with acoustic metamaterials,” Nature Reviews Materials, vol. 1, 16001, 2016, doi: 10.1038/natrevmats.2016.1.

[7] L. Huang et al., “Acoustic resonances in non-Hermitian open systems,” Nature Reviews Physics, vol. 6, pp. 11-27, 2024, doi: 10.1038/s42254-023-00659-z.

[8] Y. Ashida, Z. Gong, and M. Ueda, “Non-Hermitian physics,” Advances in Physics, vol. 69, no. 3, pp. 249-435, 2020, doi: 10.1080/00018732.2021.1876991.

[9] R. Fleury, D. Sounas, and A. Alù, “An invisible acoustic sensor based on parity-time symmetry,”

Nature Communications, vol. 6, 5905, 2015, doi: 10.1038/ncomms6905.

[10] C. Shi et al., "Accessing the exceptional points of parity-time symmetric acoustics," Nature Communications, vol. 7, 11110, 2016, doi: 10.1038/ncomms11110.

[11] K. Ding, G. Ma, M. Xiao, Z. Q. Zhang, and C. T. Chan, "Emergence, coalescence, and topological properties of multiple exceptional points and their experimental realization," Physical Review X, vol. 6, 021007, 2016, doi: 10.1103/PhysRevX.6.021007.

[12] K. Ding, G. Ma, Z. Q. Zhang, and C. T. Chan, "Experimental demonstration of an anisotropic exceptional point," Physical Review Letters, vol. 121, 085702, 2018, doi: 10.1103/PhysRevLett.121.085702.

[13] V. Igoshin, M. Tsimokha, A. Nikitina, M. Petrov, I. Toftul, and K. Frizyuk, "Exceptional points in a single open acoustic resonator due to symmetry breaking," Physical Review B, vol. 109, 144102, 2024, doi: 10.1103/PhysRevB.109.144102.

[14] I. D. Toftul, K. Y. Bliokh, M. I. Petrov, and F. Nori, "Acoustic radiation force and torque on small particles as measures of the canonical momentum and spin densities," Physical Review Letters, vol. 123, 183901, 2019, doi: 10.1103/PhysRevLett.123.183901.

[15] L. P. Gor'kov, "On the forces acting on a small particle in an acoustical field in an ideal fluid," Soviet Physics Doklady, vol. 6, pp. 773-775, 1962.

[16] M. Settnes and H. Bruus, "Forces acting on a small particle in an acoustical field in a viscous fluid," Physical Review E, vol. 85, 016327, 2012, doi: 10.1103/PhysRevE.85.016327.

[17] J. T. Karlsen and H. Bruus, "Forces acting on a small particle in an acoustical field in a thermoviscous fluid," Physical Review E, vol. 92, 043010, 2015, doi: 10.1103/PhysRevE.92.043010.

[18] P. B. Muller, R. Barnkob, M. J. H. Jensen, and H. Bruus, "A numerical study of microparticle acoustophoresis driven by acoustic radiation forces and streaming-induced drag forces," Lab on a Chip, vol. 12, pp. 4617-4627, 2012, doi: 10.1039/C2LC40612H.